Article:

Structural and Thermochemical Studies of Pyrrolidine borane and Piperidine borane by Gas Electron Diffraction and Quantum Chemical Calculations

Aliyu M. Ja'o,[1] Derek A. Wann,[2] Conor D. Rankine,[2] João P. F. Nunes,[2] Jean-Claude Guillemin[3] and Sarah L. Masters[1*]

[1] School of Physical and Chemical Sciences, University of Canterbury, Private Bag 4100, Christchurch 8140, New Zealand

[2] Department of Chemistry, University of York, Heslington, York, YO10 5DD, United Kingdom

[3] Univ Rennes, École Nationale Supérieure de Chimie de Rennes, CNRS, ISCR – UMR6226, F-35000 Rennes, France

*Correspondence: sarah.masters@canterbury.ac.nz

Abstract

The gaseous structures, thermochemical properties and dehydrogenation reaction energy profiles of the borane complexes of pyrrolidine and piperidine have been investigated using gas electron diffraction (GED) and state-of-the-art computational methods. These complexes are of interest because of their potential as hydrogen storage materials for future onboard transport applications. A comparative structural and thermochemical analysis revealed structures with a slight difference in the essential B–N bond length, with the piperidine borane having a longer bond even though it has a stronger B–N bond according to predicted bond dissociation energies, a trend common with amine boranes. To identify the most favourable dehydrogenation pathway, BH_3-catalysed and uncatalysed dehydrogenation channels have been explored, where the former has been shown to be the favourable process for both complexes. The energy requirements for the hydrogen release reactions are expected to be minimal as evidenced from the calculated dehydrogenation reaction energies, implying their suitability for onboard chemical hydrogen storage.

Keywords: Hydrogen storage; Dehydrogenation; Amine boranes; Gas electron diffraction.

Introduction

Cyclic amine boranes (CABs) represent a class of single-nitrogen-containing donor-acceptor saturated complexes with the general formula $C_nH_{2n+1}N \cdot BX_3$ ($n = 2$–7, X = H, CH_3, F, Cl, Br, I). They are formed by coordinating a cyclic amine with a borane group, resulting in the formation of a dative B–N bond. They have found application as precursors in ceramic production[1,2] and as candidates for onboard chemical hydrogen storage.[3-7] Although closely-related linear analogues, such as ammonia borane (NH_3BH_3)[8-16] and alkyl amine boranes,[17-28] are well characterised, very few CABs have been studied both in terms of their structure and chemical properties. The first CAB to be synthesised was the three-membered aziridine borane;[29-31] the crystal structure was determined subsequently,[32] and the complex was later characterised by NMR and IR techniques[33] as well as low-level *ab initio* and semi-empirical methods.[34] Microwave spectroscopy (MWS) was later employed to study the barrier to internal rotation and gas-phase structure.[35] A four-membered azetidine borane (AZB) has been studied using Fourier transform ion cyclotron resonance (FT-ICR) spectrometry complemented by theoretical calculations; in these studies, AZB was found to release dihydrogen upon protonation, highlighting its potential as a future hydrogen storage material.[5] Recently, its potential as a stereoselective functionalisation agent was demonstrated,[36] and its thermal dehydrogenation in the gas phase was observed *via* GED.[37] An *ab initio* study on a series of four CABs [$C_nH_{2n+1}N \cdot BH_3$ ($n = 2$–5)] indicated their ability to release one molecule of hydrogen in a near thermoneutral process,[6, 7] an essential requirement for onboard hydrogen generation in fuel cell vehicles. Although CABs have low hydrogen content compared to NH_3BH_3, they may possess favourable thermochemical and kinetic properties necessary for the effective dehydrogenation/hydrogenation cycle. This is because theoretical evidence based on high-level calculations has shown that alkyl substitution on the nitrogen centre reduces the exothermic nature of hydrogen release reactions, thus making the reactions more thermoneutral.[23, 27] Minimising the energy requirement for dehydrogenation/hydrogenation cycles is essential for on-board hydrogen storage applications. The thermochemistry of donor-acceptor complexes is crucial to the understanding of their behaviour in terms of the dehydrogenation as well as the regeneration of the lost fuel.[38] Because donor-acceptor complexes are characterised by relatively weak dative bonds,[39] knowledge of the dative bond dissociation energy becomes important so as to allow an easy comparison with the energy barrier for the hydrogen release reactions. This is to identify which of dissociation or dehydrogenation will be favoured. While hydrogen storage compounds such as boranes and

alanes have the ability to release hydrogen under a variety of conditions,[16, 40-44] regeneration of the lost fuel remains an issue. Therefore, finding ideal compounds with favourable thermochemistry still remains a challenge for researchers.[13]

To have a deep insight into the chemistry of the dehydrogenation/hydrogenation cycle, it is necessary to explore the structure and to use state-of-the-art computational methods to predict the thermochemical properties and reaction pathways leading to the dihydrogen generation. We have employed GED to determine the structures of the borane complexes of pyrrolidine (**PYB**; Figure 1) and piperidine (**PIB**; Figure 2). By utilising coupled-cluster [CCSD(T)] calculations with extrapolation to the complete basis set limit (CBS), hereafter denoted CCSD(T)/CBS, we have investigated the thermochemical properties associated with the hydrogen storage potentials of these complexes. This method has been shown to yield thermochemical accuracy comparable to experiment.[45] We expect this work to inform future investigations of closely related compounds with potential hydrogen storage capability.
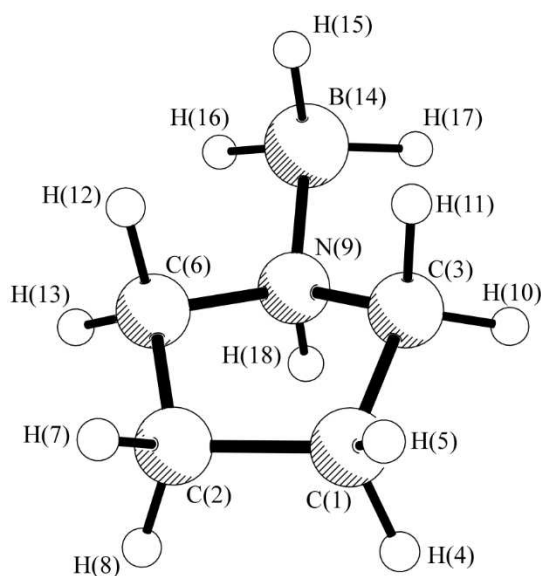

Figure 1: The lowest-energy ground-state structure of **PYB** showing the atom numbering.
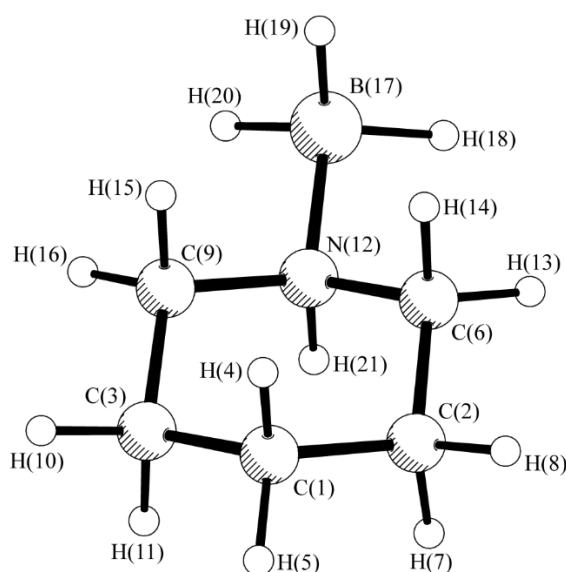
Figure 2: The lowest-energy ground-state structure of **PIB** showing the atom numbering.

Experimental and Computational Methods

Synthesis

PYB and **PIB** were synthesised according to literature methods[4, 35] and the purity was checked using ^{1}H, ^{13}C and ^{15}B NMR spectroscopy. The samples were provided for use in the GED apparatus without further purification.

Gas Electron Diffraction

GED data were acquired using the University of York gas electron diffractometer.[46] An accelerating voltage of around 42.2 keV was used, giving an electron wavelength of approximately 6.0 pm. Electron-sensitive image plates were used to record the scattering intensities. Sample/nozzle temperatures and nozzle-to-image-plate distances are given in the Supplementary Information (SI, Table S1). The data collection procedures for the compounds are described in detail in the SI. A flatbed image plate scanner (Fuji BAS1800II) was used to digitise the scattering intensities recorded on the image plates. The digitised scattering intensities were reduced to molecular-scattering intensity curves using an azimuthal averaging routine implemented in the in-house developed data extraction package *xtract*.[47] The least-squares refinement processes were carried out using the *ed@ed* program (version 2.3)[48] employing the scattering factors of Ross *et al.*[49] Weighting points for the off-diagonal weight matrices, correlation parameters and scale factors are also given

in Table S1; the least-squares correlation matrices for the refinements are provided in Tables S2 and S3.

Computational Methods

All electronic structure calculations were carried out using the GAUSSIAN 09[50] and NWCHEM[51] software suites. NWCHEM calculations were carried out using the supercomputing resources of the New Zealand eScience Infrastructure (NeSI). To incorporate the effects of electron correlation on the geometrical parameters, a series of calculations using second-order Møller-Plesset (MP2) perturbation theory[52] and the hybrid meta exchange-correlation functional (M06-2X)[53] were carried out with Pople (6-31G*, 6-311G*, 6-311+G*)[54-57] and Dunning augmented correlation-consistent (aug-cc-pVDZ, cc-pVTZ and aug-cc-pVTZ)[58] basis sets. The nature of the stationary points on the potential energy surfaces were confirmed by frequency calculations. All MP2 methods used the frozen-core approximation.

Analytic second derivatives of the energy with respect to nuclear coordinates calculated at the MP2/6-311+G* and M06-2X/aug-cc-pVTZ level of theories gave the force fields which were then used in the SHRINK[59, 60] program to provide estimates of the amplitudes of vibration (u) and perpendicular distance corrections (k) for use in the GED refinements.

Transition-state structures for the compounds along the dehydrogenation reaction pathways were obtained using the synchronous transit-guided quasi-Newton (STQN) method.[61] For the BH_3-catalysed reaction pathway, STQN was not used to predict the transition-state structure because of the numerous molecules on the pathway. The transition structures in this case were obtained by normal eigenvalue-following, *i.e.* following the reaction path from the equilibrium geometry to the transition structure by specifying which vibrational mode should lead to a reaction, given sufficient kinetic energy. To ascertain the identity of the relevant transition structures, intrinsic reaction coordinate (IRC) calculations[62] were also undertaken at the B3LYP/6-31G* level. The calculated Cartesian coordinates for all the molecules are provided in the SI (Tables S4–S15).

The thermochemical parameters at 298.15 K were calculated at CCSD(T)/CBS level and also with the composite CBS–QB3 method, employing the total atomisation energies and heat of formation as described by Curtiss *et al.*[63] This method predicts thermochemical properties with chemical accuracy with previous tests reporting the mean absolute deviation of less than 5.27 kJ/mol.[38] For the CCSD(T)/CBS method, the correlation-consistent cc-

pVnZ basis sets of Dunning,[64] with n = D, T, and Q, have been used to extrapolate the CCSD(T) energies to the complete basis set (CBS) limit by the use of the mixed Gaussian/exponential expression (Equation 1) suggested by Peterson *et al.*[45] where n = 2 (cc-pVDZ), 3 (cc-pVTZ), and 4 (cc-pVQZ).

$$E(\text{n}) = E_{\text{CBS}} + Be^{-(n-1)} + Ce^{-(n-1)^2} \qquad 1$$

This extrapolation method has been shown to yield atomisation energies in close agreement with experiment (by comparison to other extrapolation approaches) with input up to n = 4. The zero-point energies (ΔE_{ZPE}) and thermal corrections for the enthalpy, entropy and Gibbs free energy were obtained at the MP2 level with the cc-pVTZ basis set. The calculated energies and corrections for enthalpy (H), Gibbs free energy (G) and zero-point energies used in the calculation of the thermochemical properties are provided in the SI (Tables S16–S19).

Results and Discussion

Ab Initio **Calculations**

The equilibrium structures for **PYB** and **PIB** with the atom numbering, calculated using the M06-2X method, are shown in Figures 1 and 2, respectively. **PYB** and **PIB** are C_s-symmetric molecules in which the BH$_3$ is found in an equatorial conformation. To analyse the effect of basis set size on the geometry of the systems, the M06-2X level of theory was employed with assorted basis sets possessing additional diffuse and polarization functions. The observed changes in geometry with improved basis set were used to calculate the restraints for use in a least-squares structural refinement with the SARACEN method.[65-67] Selected parameters from the equilibrium geometries are shown in Tables 1 and 2. All the calculated bond lengths in both compounds are similar to within ~ 1 pm. It was observed that the change in the basis sets used did not yield any significant differences in the geometrical parameters. The B–N bond lengths are comparable to that of AZB. It can therefore be said that the ring size does not significantly affect the B–N bond distance. The small difference in rB–N between **PYB** and **PIB** is unexpected because the ring strain in **PYB** is more pronounced than in **PIB** which could be expected to elongate rB–N based on the Gillespie's valence shell electron pair repulsion model (VSEPR).[68-71] However, the presence of a ring carbon atom [C(1), Figure 2] in the same plane as the B–N bond (opposite the N) which is absent in **PYB**, may also prompt a repulsion along the plane of the C…N–

6

B interaction (the mirror plane of the molecule). This would result in the lengthening of the B–N bond in **PIB** by pushing the BH_3 unit further away from the ring to minimise the repulsion. The latter rationale, also based on VSEPR, is then expected to dominate. $\angle$C–N–B in **PYB** (similar to AZB) was wider than in **PIB** by ~3° which can be rationalised by the ring strain and geometry in **PYB** (5 *vs* 6 membered ring). The $\angle$N–B–H values for both **PYB** and **PIB** agree excellently with each other with the ring size having no effect on the bond angle. Generally, it can be said that both **PYB** and **PIB** have been adequately described by the respective level of theories used.

Table 1: Selected optimised parameters for **PYB** using the M06-2X method with different basis sets.

Parameter[a]	M06-2X		
	aug-cc-pVDZ	cc-pVTZ	aug-cc-pVTZ
rB–N	162.1	162.2	162.2
rN–C	148.3	148.1	148.1
rC–C	153.5	153.2	153.2
rN–H	102.1	101.8	101.8
rB–H av	121.9	120.9	120.9
rC–H av	109.5	108.8	108.8
∠C–N–B	114.9	114.9	114.9
∠C–N–C	103.7	103.5	103.4
∠N–B–H av	105.4	105.4	105.4
ϕC–C–N–B	-165.2	-165.4	-165.3

[a] Distances in pm; Angles in °.

Table 2: Selected optimised parameters for **PIB** using the M06-2X method with different basis sets.

Parameter[a]	M06-2X		
	aug-cc-pVDZ	cc-pVTZ	aug-cc-pVTZ
rB–N	162.6	162.9	162.8
rN–C	148.4	148.2	148.2
rC–C	152.4	152.1	152.1
rC…N	293.9	293.6	293.6
rN–H	102.2	101.9	101.8
rB–H av	121.9	120.9	120.9
rC–H av	109.8	109.5	109.1
∠C–N–B	112.0	111.7	111.9
∠C–N–C	111.1	111.1	111.1
∠C…N–B	155.2	154.8	154.8
∠N–B–H av	105.4	105.4	105.5
ϕC–C–N–B	177.8	178.3	178.3

[a] Distances in pm; Angles in °.

GED Refinement

Parameterized molecular models describing the structures of **PYB** and **PIB** for the SARACEN r_{h1}-type[72] refinements were constructed based on the C_s equilibrium geometries predicted at the M06-2x/aug-cc-pVTZ level. The equilibrium geometries were described using 20 independent parameters (6 bond lengths, 8 bond angles and 6 dihedral angles) for **PYB** and 24 independent parameters (7 bond lengths, 11 bond angles and 6 dihedral angles) for **PIB**. Theoretical Cartesian force fields were converted into force fields defined by a set of symmetry coordinates using the SHRINK program,[59, 73] yielding initial amplitudes of vibration (u_{h1}) and curvilinear corrections (k_{h1}) for the compounds. The SARACEN[65-67] refinement method was employed in the least-squares refinement; flexible restraints were determined from the theoretical parameters (Tables 1 and 2). All parameters for both **PYB** and **PIB** were refined and, unlike AZB, no *in situ* dehydrogenation was observed at the temperature of the experiments, allowing the gas-phase structures of **PYB** and **PIB** to be determined cleanly. It is not clear why dehydrogenation was not observed in these cases, given the predicted reaction energy pathways and thermochemical parameters (discussed below) which suggest a favourable hydrogen release reaction like that of AZB. The lack of dehydrogenation could be due to a decrease in the steric hindrance with an increase in ring size from AZB to **PYB** and **PIB.** Also, because the temperature needed to vaporise AZB is lower than for both **PYB** and **PIB**, it is expected that the former should have a slightly lower vapour pressure than the latter. For AZB, suitable vapour pressures were not obtained below the decomposition temperature contrary to **PYB** and **PIB**. That **PYB** and **PIB** are solids at STP, unlike AZB which is liquid under the same conditions, may also be another reason why it was not so easy to dehydrogenate either under the conditions of the experiment. Salient refined structural parameters are provided in Table 3 together with the applied restraints and the parameters from the highest-level equilibrium geometries (M06-2X/aug-cc-pVTZ). The full lists of the refined structural parameters are tabulated in the SI (Tables S20 and S21). Restraints were added to parameters that do not refine freely. All relevant vibrational amplitudes were refined and are reported in the SI (Tables S22 and S23). The success of the final refinements for both compounds can be assessed qualitatively by examining the radial distribution curves (RDC) for both compounds as shown in Figures 3 and 4, and quantitatively by an R_G factor of 6.9 % (for **PYB**) and 3.3 % (for **PIB**). The molecular scattering intensity curves (MICs) are shown in the SI (Figures S1 and S2).

Calculations were also been performed using MP2/6-311+G* methods. For **PIB** a C_s structure was returned as the energy minimum on the PES, however for **PYB** a C_1 structure was obtained. We tried various approaches to obtain a C_s geometry for **PYB** however all resulted in an imaginary frequency that, when animated, indicated significant ring distortion. We performed refinements of the GED data using models of C_s symmetry for **PIB** and C_1 symmetry for **PYB** using the MP2 structure as a starting point and generating all vibrational corrections and restraints from this series of calculations. The refinement for the C_1 structure of **PYB** had 12 more parameters compared to the model with C_s symmetry. The refinement did not give a good fit between the model and the experiment, yielding an R_G factor of 28.8%. The results from the refinement of **PIB** are very similar to those from the structure reported above (R_G = 3.4 *vs* 3.3%). The calculated coordinates for the MP2 calculations are provided in the SI (Tables S24-S26 for **PYB** and Tables S28-S30 for **PIB** respectively). The MICs and RDCs are also shown in the SI (Figures S7-S8 for **PYB** and Figures S9-S10 for **PIB** respectively). The least-squares correlation matrix for the successful **PIB** refinement (using MP2/6-311+G* geometry) is provided in Table S27 while the full lists of the refined structural parameters and amplitudes of vibration are tabulated in Tables S31-S32.

Table 3: Selected refined (r_{h1}) and calculated (r_e; M06-2X/aug-cc-pVTZ) geometric parameters for **PYB** and **PIB**.

Parameter[a]	PYB			PIB		
	Theory (r_e)	Experiment (r_{h1})	Restraint	Theory (r_e)	Experiment (r_{h1})	Restraint
rB–N	162.2	162.8(5)	162.2(5)	162.8	163.5(3)	162.8(3)
rN–C	148.1	147.9(3)	148.1(4)	148.2	148.3(2)	148.2(2)
∠C–N–B	114.9	114.9(2)	114.9(2)	111.9	112.0(3)	111.9(4)
∠C–N–C[b]	103.4	103.9(7)	-	111.1	110.8(3)	-
ϕC–C–N–B	–165.3	–165.0(4)	–165.3(4)	178.3	178.1(5)	178.3(5)

[a] Distances in pm; Angles in °.

[b] ∠C–N–C is a dependent parameter. Digits in parentheses are the estimated standard deviation of the last digits expressed as 2σ.

From the RDCs, it is evident that the experimental and theoretical data agree with each other for both molecules. The parameters from both theory and experiment for both compounds are comparable, giving confidence in the computational methods chosen. The dehydrogenation of AZB which resulted in the GED refinement yielding a higher R_G value (15.0 %) and consequently a reasonably inaccurate structure means that a comparison between the molecular structure of AZB with those of **PYB** and **PIB** cannot be made for the experimental data. The experimental value of rB–N for **PIB** is longer than that of **PYB** by 0.7 pm. This is expected because dative bond lengths have been known to be sensitive to inductive effects when the size or number of electron donating groups is increased on the nitrogen containing ring.[74] However, this is unlikely to be responsible for the bond elongation in this case. Rather, the additional –CH$_2$ group on the ring in **PIB** is likely responsible for this bond elongation due to the changes in geometry around the N centre. For instance, the $\angle$C–N–C increases from 103.9(7)° in **PYB** to 110.1(3)° in **PIB**. A similar trend in the B–N bond length increase has been observed for the aliphatic series Me$_n$H$_{3-n}$N·BH$_3$ (n = 1–3), where the B–N bond lengthened upon successive methylation at the nitrogen centre.[24]

The experimental value of rN–C for **PYB** [147.9(3) pm] is similar to that obtained for N–chloropyrrolidine [147.6(5) pm] and an earlier[75] [147.7(8) pm] and later[76] [147.9(9) pm] value for N–nitropyrrolidine, but longer (by 2.4 pm) than that of N–methylpyrrolidine [145.5(3) pm].[77] It can therefore be argued that a substituent effect in pyrrolidines is an indicator of rN–C only when electron donating groups are covalently bonded to the nitrogen (external to the ring rather than on the ring itself) as in the latter case. Another example is rN–C in **PIB** having excellent agreement with the M06-2X/aug-cc-pVTZ value [148.3(2) pm cf. 148.2 pm]. This is significantly longer than that in N–cyclohexylpiperidine[78] [146.0(3) pm].
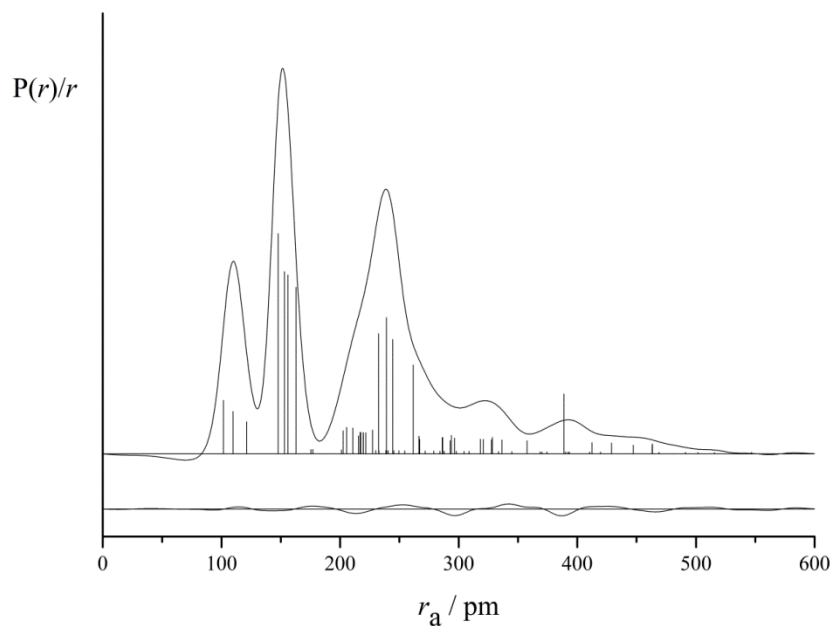
Figure 3: Experimental and difference (experimental minus theoretical) RDCs for the GED refinement of **PYB**. Before Fourier inversion, the data were multiplied by $s \cdot \exp(-0.00002s^2)/(Z_C - f_C)(Z_N - f_N)$.
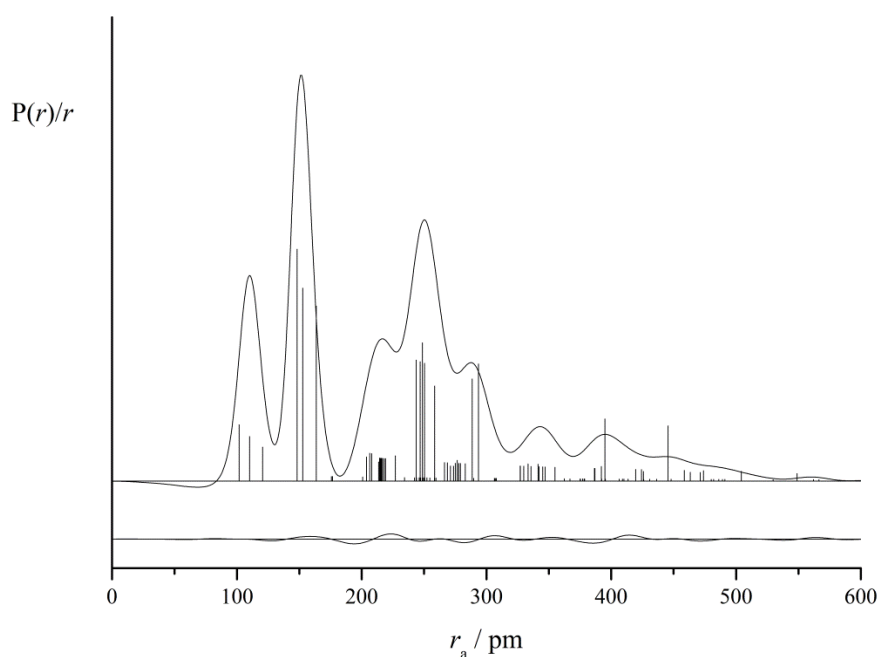

Figure 4: Experimental and difference (experimental minus theoretical) RDCs for the GED refinement of **PIB**. Before Fourier inversion, the data were multiplied by $s \cdot \exp(-0.00002s^2)/(Z_C - f_C)(Z_N - f_N)$.

Reaction pathways for the dehydrogenation reactions

The energy profile diagrams for the dehydrogenation reactions in the absence/presence of BH$_3$ catalyst for **PYB** and **PIB** are depicted in Figures 5 and 6 respectively. The transition state (**TS**) structures along the uncatalysed (**TS1**) and catalysed (**TS2**) dehydrogenation pathways for both **PYB** and **PIB** are also shown in Figures 7–10. Passing through **TS1** (without the catalyst) indicates an activation barrier larger than the B–N bond dissociation energy (B–N$_{BDE}$) predicted at CBS–QB3; the same was found for AZB. This suggests that the dissociation of the complexes may be favoured over the dehydrogenation reaction. In the case of NH$_3$BH$_3$, it has been reported that the BH$_3$ generated from the B–N bond cleavage acted as a bifunctional catalyst in the hydrogen release reactions, reducing the barrier from 201.3 to 25.1 kJ mol^{-1} at the CCSD(T)/CBS level of theory.[79] A similar trend was observed for NH$_3$AlH$_3$, with AlH$_3$ serving as a catalyst in the dehydrogenation process.[41] A theoretical study[6, 7] at the G4MP2 level of theory on the dehydrogenation pathway with/without BH$_3$ as a catalyst for a series of cyclic amine boranes [C$_n$H$_{2n+1}$N·BH$_3$ ($n = 2$–5)] revealed the same pattern.
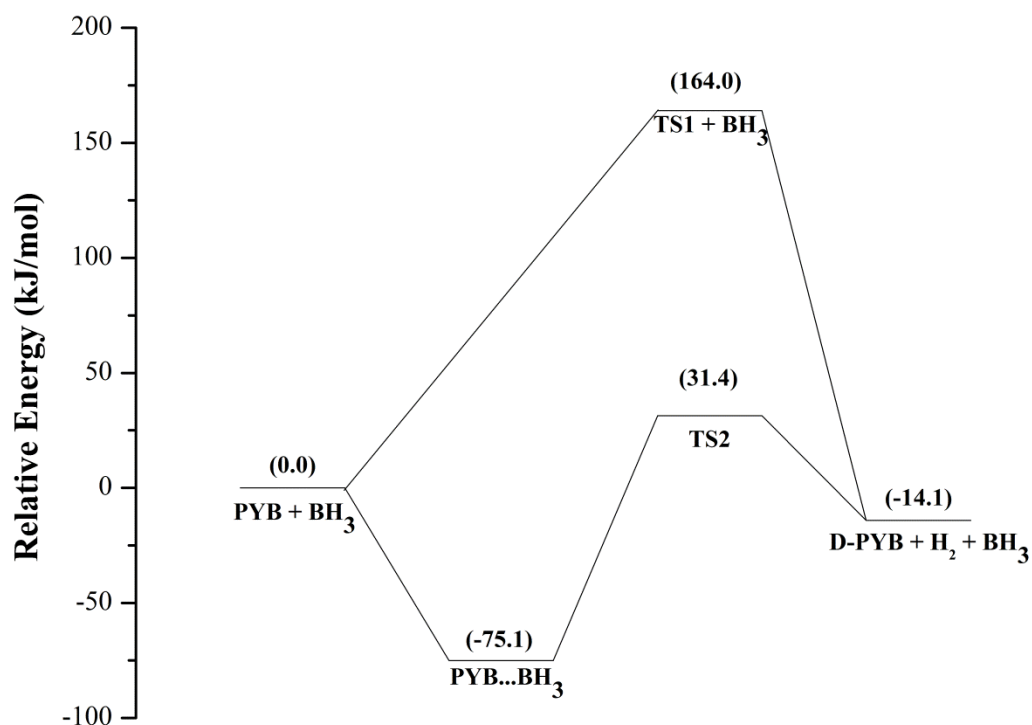

Figure 5: Energy profile for the dehydrogenation of **PYB** without (*via* **TS1**) and with (*via* **TS2**) the presence of BH$_3$ at 298.15 K using CBS–QB3. Relative energies (in brackets) in kJ mol^{-1}.
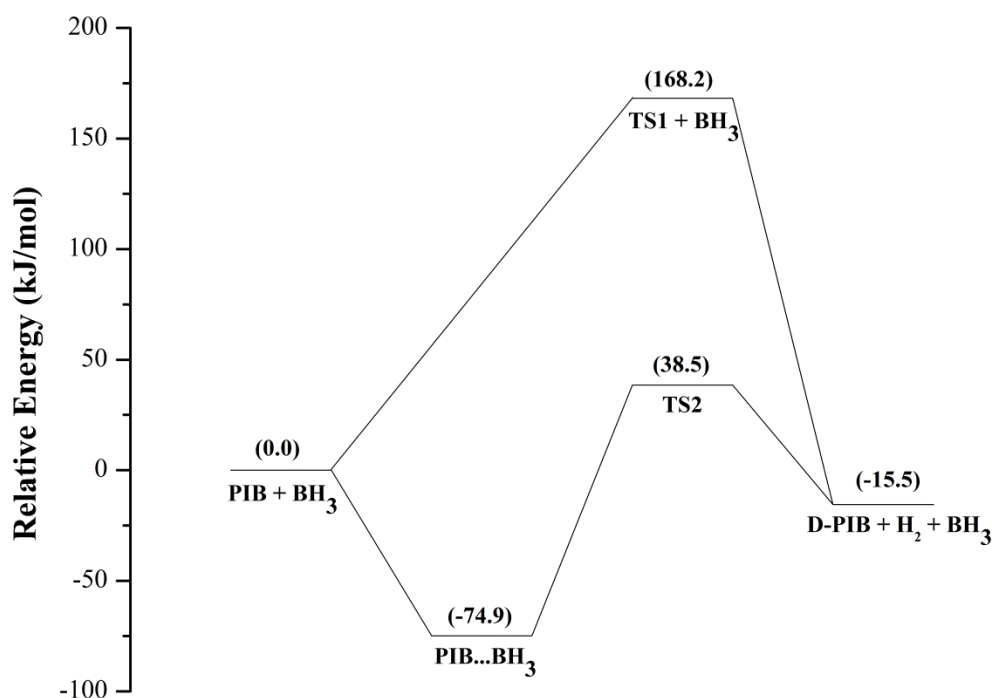
Figure 6: Energy profile for the dehydrogenation of **PIB** without (*via* **TS1**) and with (*via* **TS2**) the presence of BH_3 at 298.15 K using CBS–QB3. Relative energies (in parenthesis) in kJ mol^{-1}.

Therefore, the reaction pathways for the hydrogen release reaction using BH_3 as a catalyst *via* **TS2** were also investigated. An interaction of BH_3 with **PYB** and **PIB** produced barrier-free adducts, **PYB…BH₃** (for **PYB**, Figure S3) and **PIB…BH₃** (for **PIB**, Figure S4), which were found to be stabilized relative to the reactants by 75.1 and 74.9 kJ mol^{-1}, respectively. Compared to AZB…BH_3, these barrier-free adducts are slightly more stable. The **TS2** structures were then located with a reduced barrier of 31.4 (**PYB**) and 38.5 (**PIB**) kJ mol^{-1} (again, slightly lower than that for AZB, and far below the dissociation energies shown in Table 4). The dehydrogenation reactions then proceed to form the dehydrogenated compounds **D–PYB** (for **PYB**, Figure S5) and **D–PIB** (for **PIB**, Figure S6). These results are consistent with that of AZB and those obtained in the literature at G4MP2 for similar complexes[7] and have also demonstrated the active participation and suitability of BH_3 to act as a Lewis acid catalyst in a favoured dehydrogenation process similar to AZB.
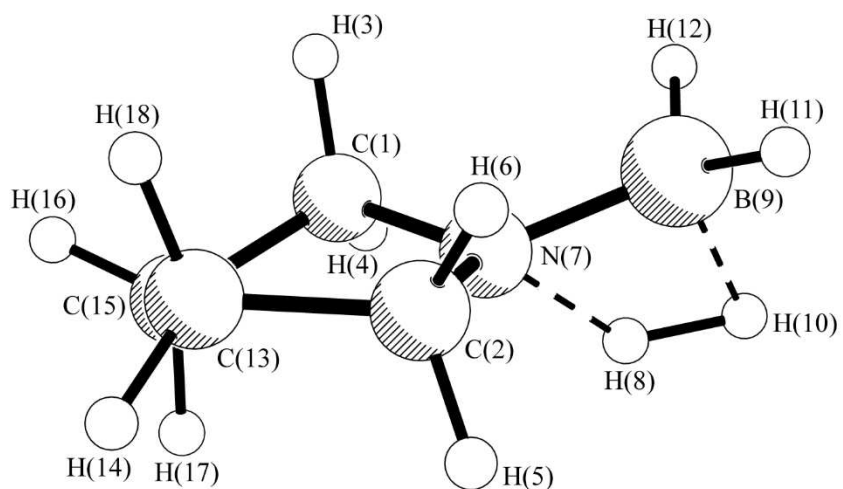
Figure 7: The transition-state structure for the dehydrogenation of **PYB** in the absence of BH$_3$ catalyst (**TS1**).
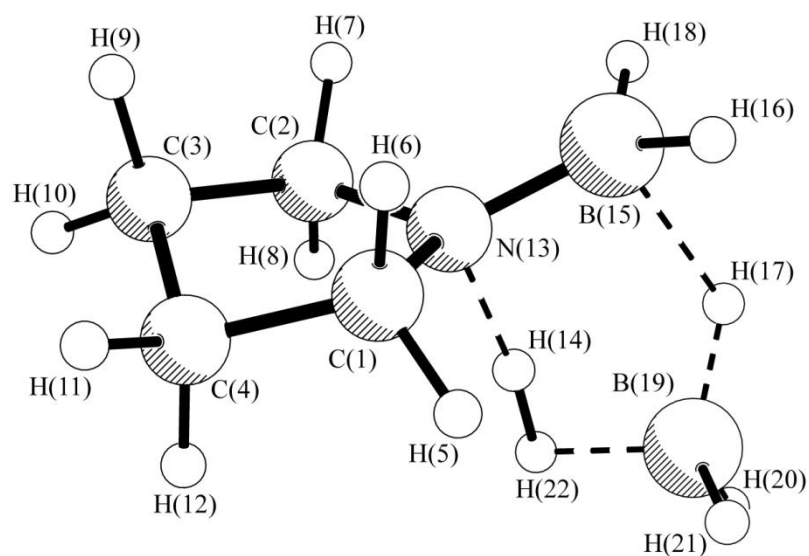

Figure 8: The transition-state structure for the dehydrogenation of **PYB** in the presence of BH$_3$ catalyst (**TS2**).
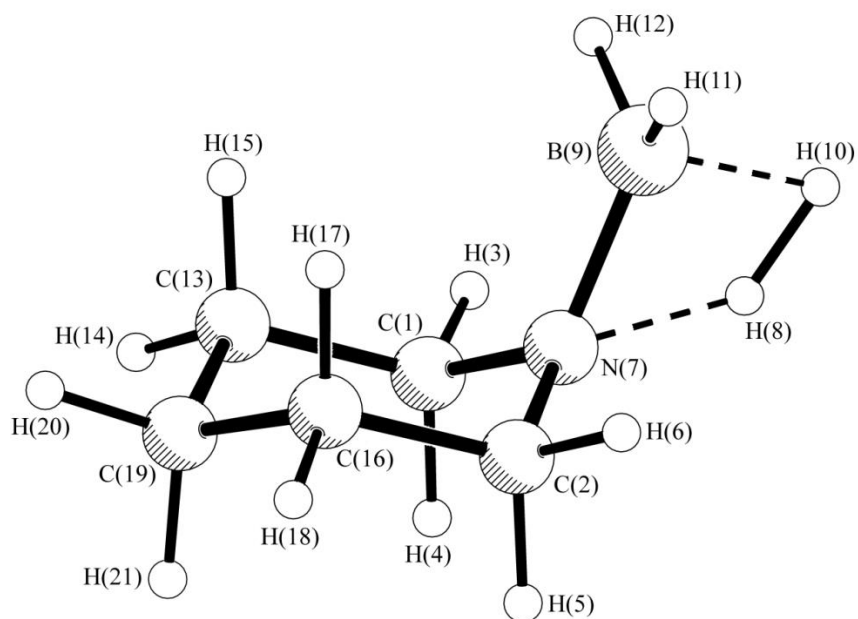
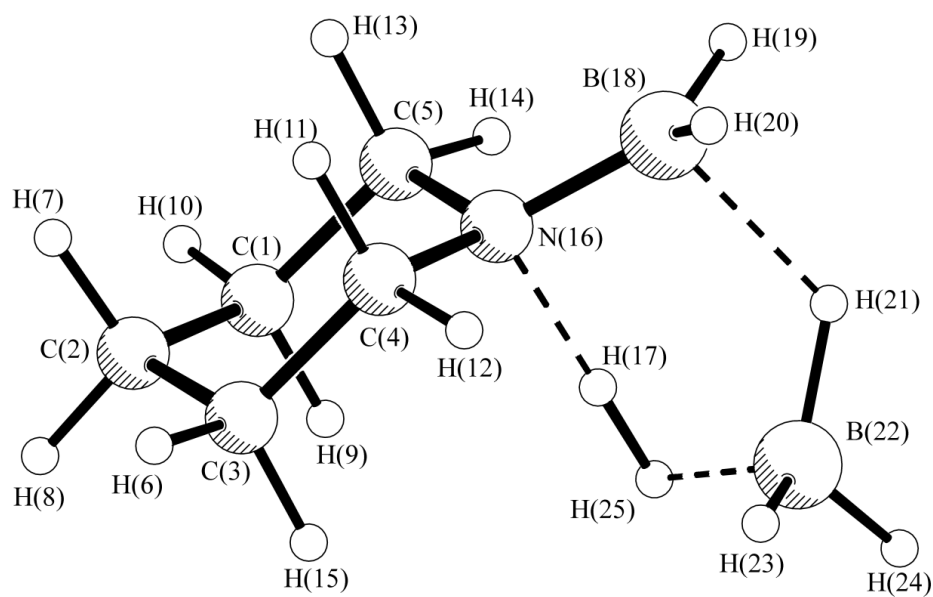Figure 9: The transition-state structure for the dehydrogenation of **PIB** in the absence of BH$_3$ catalyst (**TS1**).

Figure 10: The transition-state structure for the dehydrogenation of **PIB** in the presence of BH$_3$ catalyst (**TS2**).

Thermochemical studies

The dehydrogenation enthalpy (ΔH_r), Gibbs free energy (ΔG_r) and entropy (ΔS_r) as well as the B–N bond dissociation energy (B–N$_{BDE}$) predicted at CCSD(T)/CBS and CBS–QB3 levels of theory and at 298.15 K are presented in Table 4. To simplify this discussion, only the more accurate CCSD(T)/CBS method will be discussed especially given that, for the parameters (except B–N$_{BDE}$ and ΔS_r), the level of agreement across the methods is within 4–8 kJ mol^{-1}. There is an increase in the B–N$_{BDE}$ from AZB (161.2 kJ/mol)[37] to **PYB** to **PIB** indicating that the strength of the dative bond increases with increase in ring size. This means it is more likely for **PYB** to dissociate than **PIB** even though the B–N bond length in **PIB** is longer than in **PYB**. This observation resembles the experimental values for rB–N [163.3(7) pm and 164.2(4) pm][24] and corresponding B–N$_{BDE}$ [146.4(1) kJ mol^{-1} and 152.3(1) kJ mol^{-1}][74] for methyl and dimethyl amine boranes. This contradicts the assumption that a shorter bond is stronger than a longer bond.

The hydrogen release reactions for both compounds have enthalpies that are exothermic and close to thermoneutral with that for **PIB** being less exothermic. Therefore, the energy required to release a hydrogen molecule is expected to be minimal. It is surprising that, given that the reaction pathways for both **PYB** and **PIB** have slightly lower barriers than AZB, the latter seems to have a more thermoneutral dehydrogenation reaction as evident from the enthalpy values. However, the ΔG_r values for **PYB** and **PIB** at CCSD(T)/CBS level, being lower than for AZB, support the earlier observations from the reaction energy pathway studies discussed above. The calculated ΔH_r values for **PYB** and **PIB** are similar to that of dimethylamine borane [($CH_3)_2NHBH_3$, –7.5 kJ mol^{-1})] but lower than those obtained for ammonia borane (NH_3BH_3, –21.3 kJ mol^{-1}) and methylamine borane ($CH_3NH_2BH_3$, –14.3 kJ mol^{-1}) using the same computational methods. This suggests that the dehydrogenation reactions for **PYB** and **PIB** are less exothermic than NH_3BH_3 and $CH_3NH_2BH_3$. The predicted ΔH_r value for NH_3BH_3 was supported by the experimental observation of its dehydrogenation process *via* thermal decomposition, which was reported to occur under mild conditions and below its melting point temperature of 385 K. Based on this observation and coupled with the predicted values above, the dehydrogenation reaction for both **PYB** and **PIB** is expected to take place under milder conditions than NH_3BH_3. The ΔG_r values show that the dehydrogenation reactions in **PYB** and **PIB** are spontaneous, feasible and exergonic under standard conditions. These values are larger than the

calculated value for aziridine borane (-35.8 kJ mol^{-1}) at B3LYP/aug-cc-pVTZ level.[4] The ΔS_r for NH_3BH_3 (+125.0 J/mol/K) calculated at MP2/cc-pVTZ level[38] is comparable to the values calculated for **PYB** and **PIB** but slightly higher than that of AZB (117.0 J K^{-1} mol^{-1}). This may indicate that NH_3BH_3, **PYB** and **PIB**, being solids, are likely to have their dehydrogenation taking place in the gas-phase similar to AZB which exists as a liquid in its pure form. However, unlike AZB, the *in-situ* dehydrogenation of **PYB** and **PIB** was not observed experimentally as explained above.

Table 4: Thermochemical parameters for **PYB** and **PIB** predicted at 298.15 K at the CCSD(T)/CBS and CBS–QB3 levels of theory.

Property[a]	PYB		PIB	
	CCSDT(T)/CBS	CBS–QB3	CCSDT(T)/CBS	CBS–QB3
B–N$_{BDE}$	+179.6	+157.9	+189.6	+160.2
ΔH_r	–8.2	–11.1	–6.2	–12.9
ΔG_r	–46.1	–46.5	–42.1	–48.6
ΔS_r	+127.1	+117.2	+120.5	+121.3

[a] Units in kJ mol^{-1} except ΔS_r which is in J K^{-1} mol^{-1}.

Conclusion

The gas-phase molecular structures of **PYB** and **PIB** have been determined for the first time using GED and complementary theoretical calculations, while their hydrogen storage capabilities have been demonstrated from a theoretical perspective. It was found that the B–N internuclear distance in **PYB**, although similar to that in AZB, is shorter than that of **PIB**. This trend is similar to that reported for linear amine boranes Me$_n$H$_{3-n}$N·BH$_3$ (n = 1–3).[24] The B–N$_{BDE}$ values indicate an increase in the strength of the B–N bond with increase in ring size, even though a cursory examination of the bond lengths would suggest otherwise. Unlike AZB, these compounds did not undergo *in situ* dehydrogenation during the GED experiment, even though the operating temperatures during data acquisition were

higher than that used for AZB. Nonetheless, their calculated thermochemical properties and reaction energy pathways for BH_3-catalysed hydrogen release indicate a more facile and thermoneutral process by comparison with that found for AZB.

References

1.   Goto, Y.; Sasaki, M. *Mater. Trans. JIM* **2000,** *41* (8), 1068-1072.

2.   Matizamhuka, W. R.; Sigalas, I.; Herrmann, M.; Dubronvinsky, L.; Dubrovinskaia, N.; Miyajima, N.; Mera, G.; Riedel, R. *Materials* **2011,** *4* (12), 2061-2072.

3.   Nemeth, B.; Guegan, J. P.; Veszpremi, T.; Guillemin, J.-C. *Inorg. Chem.* **2013,** *52* (1), 346-354.

4.   Németh, B.; Khater, B.; Guillemin, J.-C.; Veszprémi, T. *Inorg. Chem.* **2010,** *49* (11), 4854-4864.

5.   Abboud, J. L. M.; Németh, B.; Guillemin, J.-C.; Burk, P.; Adamson, A.; Nerut, E. R. *Chem. Eur. J.* **2012,** *18* (13), 3981-3991.

6.   Banu, T.; Sen, K.; Ghosh, D.; Debnath, T.; Das, A. K. *RSC Adv.* **2014,** *4* (3), 1352-1361.

7.   Sen, K.; Banu, T.; Debnath, T.; Ghosh, D.; Das, A. K. *RSC Adv.* **2014,** *4* (42), 21924.

8.   Umeyama, H.; Morokuma, K. *J. Am. Chem. Soc.* **1976,** *98* (23), 7208-7220.

9.   Hu, M.; Geanangel, R.; Wendlandt, W. *Thermochim. Acta* **1978,** *23* (2), 249-255.

10.   Anane, H.; Jarid, A.; Boutalib, A.; Nebot-Gil, I.; Tomás, F. *J. Mol. Struct.: THEOCHEM* **1998,** *455* (1), 51-57.

11.   Lane, C.F. Ammonia-Borane and Related N-B-H Compounds and Materials: Safety Aspects, Properties and Applications (a survey completed as part of a project for the DOE Chemical Hydrogen Storage Center of Excellence, Contract # DE-FC36-05GO15060) **2006**. Northern Arizona University, Flagstaff, AZ. Available at http://www1.eere.energy.gov/hydrogenandfuelcells/pdfs/nbh_h2_storage_survey.pdf (accessed 16/07/20).

12.   Miranda, C. R.; Ceder, G. *J. Chem. Phys.* **2007,** *126* (18), 184703.

13.   Stephens, F. H.; Pons, V.; Baker, R. T. *Dalton Trans.* **2007,** (25), 2613-2626.

14.   Bowden, M.; Autrey, T.; Brown, I.; Ryan, M. *Curr. Appl. Phys.* **2008,** *8* (3), 498-500.

15.   Staubitz, A.; Robertson, A. P.; Manners, I. *Chem. Rev.* **2010,** *110* (7), 4079-4124.

16.   Lu, Z.-H.; Yao, Q.; Zhang, Z.; Yang, Y.; Chen, X. *J. Nanomater.* **2014,** *2014*, 729029/1-729029/12.

17. Durig, J. R.; Li, Y. S.; Odom, J. D. *J. Mol. Struct.* **1973,** *16* (3), 443-450.

18. Cassoux, P.; Kuczkowski, R. L.; Bryan, P. S.; Taylor, R. C. *Inorg. Chem.* **1975,** *14* (1), 126-129.

19. Iijima, K.; Shibata, S. *Bull. Chem. Soc. Jpn.* **1979,** *52* (3), 711-715.

20. Iijima, K.; Shibata, S. *Bull. Chem. Soc. Jpn.* **1980,** *53* (7), 1908-1913.

21. Iijima, K.; Shibata, S. *Bull. Chem. Soc. Jpn.* **1983,** *56* (7), 1891-1895.

22. Iijima, K.; Adachi, N.; Shibata, S. *Bull. Chem. Soc. Jpn.* **1984,** *57* (11), 3269-3273.

23. Sun, C.; Yao, X.; Du, A.; Li, L.; Smith, S.; Lu, G. *Phys. Chem. Chem. Phys.* **2008,** *10* (40), 6104-6106.

24. Aldridge, S.; Downs, A. J.; Tang, C. Y.; Parsons, S.; Clarke, M. C.; Johnstone, R. D. L.; Robertson, H. E.; Rankin, D. W. H.; Wann, D. A. *J. Am. Chem. Soc.* **2009,** *131* (6), 2231-2243.

25. Clippard, P. H.; Hanson, J. C.; Taylor, R. C. *J. Cryst. Mol. Struct.* **1971,** *1* (6), 363-371.

26. Hargittai, M.; Hargittai, I. *J. Mol. Struct.* **1977,** *39* (1), 79-89.

27. Grant, D. J.; Matus, M. H.; Anderson, K. D.; Camaioni, D. M.; Neufeldt, S. R.; Lane, C. F.; Dixon, D. A. *J. Phys. Chem. A.* **2009,** *113* (21), 6121-6132.

28. Bowden, M. E.; Brown, I. W.; Gainsford, G. J.; Wong, H. *Inorg. Chim. Acta* **2008,** *361* (7), 2147-2153.

29. Burg, A. B.; Good, C. D. *J. Inorg. Nucl. Chem.* **1956,** *2* (4), 237-245.

30. Akerfeldt, S.; Hellstro, M. *Acta Chem. Scand.* **1966,** *20* (5), 1418.

31. Akerfeldt, S.; Wahlberg, K.; Hellström, M. *Acta Chem. Scand.* **1969,** *23* (1), 115-l25.

32. Ringertz, H. *Acta Chem. Scand.* **1969,** *23* (1), 137-143.

33. Williams, R. *Acta Chem. Scand.* **1969,** *23* (1), 149-158.

34. Kroll, J. A.; Shillady, D. D. *J. Am. Chem. Soc.* **1973,** *95* (5), 1422-1425.

35. Konovalov, A.; Møllendal, H.; Guillemin, J.-C. *J. Phys. Chem. A.* **2009,** *113* (29), 8337-8342.

36. Andresini, M.; De Angelis, S.; Uricchio, A.; Visaggio, A.; Romanazzi, G.; Ciriaco, F.; Corriero, N.; Degennaro, L.; Luisi, R. *J. Org. Chem.* **2018,** *83* (17), 10221-10230.

37. Ja'o, A. M.; Masters, S. L.; Wann, D. A.; Rankine, C. D.; Nunes, J. P. F.; Guillemin, J.-C. *J. Phys. Chem. A.* **2019,** *123* (32), 7104-7112.

38. Matus, M. H.; Anderson, K. D.; Camaioni, D. M.; Autrey, S. T.; Dixon, D. A. *J. Phys. Chem. A.* **2007,** *111* (20), 4411-4421.

39. Gilbert, T. M. *J. Phys. Chem. A.* **2004,** *108* (13), 2550-2554.

40. Grant, D. J.; Dixon, D. A. *J. Phys. Chem. A.* **2005,** *109* (44), 10138-10147.

41. Nguyen, V. S.; Matus, M. H.; Ngan, V. T.; Nguyen, M. T.; Dixon, D. A. *J. Phys. Chem. C.* **2008,** *112* (14), 5662-5671.

42. Nguyen, V. S.; Swinnen, S.; Nguyen, M. T.; Dixon, D. A. *J. Phys. Chem. C.* **2009,** *113* (43), 18914-18926.

43. Nguyen, V. S.; Majumdar, D.; Leszczynski, J.; Nguyen, M. T. *Chem. Phys. Lett.* **2013,** *584*, 30-36.

44. Niaz, S.; Manzoor, T.; Pandith, A. H. *Renew. Sustain. Energy Rev.* **2015,** *50*, 457-469.

45. Feller, D.; Peterson, K. A.; Grant Hill, J. *J. Chem. Phys.* **2011,** *135* (4), 044102.

46. Rankine, C. D.; Nunes, J. P. F.; Lock Feixas, T.; Young, S.; Wann, D. A. A. *J. Phys. Chem. A.* **2018,** *122* (25), 5656-5665.

47. Nunes, J. P. F. Ph.D Thesis, University of York, **2017**.

48. Hinchley, S. L.; Robertson, H. E.; Borisenko, K. B.; Turner, A. R.; Johnston, B. F.; Rankin, D. W. H.; Ahmadian, M.; Jones, J. N.; Cowley, A. H. *Dalton Trans.* **2004,** (16), 2469-2476.

49. Ross, A. W.; Fink, M.; Hilderbrandt, R. *International Tables for Crystallography,* ed. Wilson, A. J. C., Kluwer Academic Publishers, Dordrecht, Boston and London, **1992,** vol. C, p. 245.

50. Frisch, M. J.; Trucks, G. W.; Schlegel, H. B.; Scuseria, G. E.; Robb, M. A.; Cheeseman, J. R.; Scalmani, G.; Barone, V.; Mennucci, B.; Petersson, G. A.; Nakatsuji, H.; Caricato, M.; Li, X.; Hratchian, H. P.; Izmaylov, A. F.; Bloino, J.; Zheng, G.; Sonnenberg, J. L.; Hada, M.; Ehara, M.; Toyota, K.; Fukuda, R.; Hasegawa, J.; Ishida, M.; Nakajima, T.; Honda, Y.; Kitao, O.; Nakai, H.; Vreven, T.; Montgomery, J. J. A.; Peralta, J. E.; Ogliaro, F.; Bearpark, M.; Heyd, J. J.; Brothers, E.; Kudin, K. N.; Staroverov, V. N.; Keith, T.; Kobayashi, R.; Normand, J.; Raghavachari, K.; Rendell, A.; Burant, J. C.; Iyengar, S. S.; Tomasi, J.; Cossi, M.; Rega, N.; Millam, J. M.; Klene, M.; Knox, J. E.;

Cross, J. B.; Bakken, V.; Adamo, C.; Jaramillo, J.; Gomperts, R.; Stratmann, R. E.; Yazyev, O.; Austin, A. J.; Cammi, R.; Pomelli, C.; Ochterski, J. W.; Martin, R. L.; Morokuma, K.; Zakrzewski, V. G.; Voth, G. A.; Salvador, P.; Dannenberg, J. J.; Dapprich, S.; Daniels, A. D.; Farkas, O.; Foresman, J. B.; Ortiz, J. V.; Cioslowski, J.; Fox, D. J. *Gaussian 09, Revision B.01, Gaussian Inc, Wallingford* **2009**.

51. Valiev, M.; Bylaska, E. J.; Govind, N.; Kowalski, K.; Straatsma, T. P.; Van Dam, H. J.; Wang, D.; Nieplocha, J.; Apra, E.; Windus, T. L. *Comp. Phys. Commun.* **2010,** *181* (9), 1477-1489.

52. Frisch, M. J.; Head-Gordon, M.; Pople, J. A. *Chem. Phys. Lett.* **1990,** *166* (3), 275-280.

53. Zhao, Y.; Truhlar, D. G. *Theo. Chem. Acc.* **2008,** *120* (1), 215-241.

54. Hehre, W. J.; Ditchfield, R.; Pople, J. A. *J. Chem. Phys.* **1972,** *56* (5), 2257-2261.

55. Krishnan, R.; Binkley, J. S.; Seeger, R.; Pople, J. A. *J. Chem. Phys.* **1980,** *72* (1), 650-654.

56. Francl, M. M.; Pietro, W. J.; Hehre, W. J.; Binkley, J. S.; Gordon, M. S.; DeFrees, D. J.; Pople, J. A. *J. Chem. Phys.* **1982,** *77* (7), 3654-3665.

57. Frisch, M. J.; Pople, J. A.; Binkley, J. S. *J. Chem. Phys.* **1984,** *80* (7), 3265-3269.

58. Woon, D. E.; Dunning J, T. H. *J. Chem. Phys.* **1995,** *103* (11), 4572-4585.

59. Sipachev, V. *J. Mol. Struct.: THEOCHEM* **1985,** *121*, 143-151.

60. Sipachev, V. *J. Mol. Struct.* **2001,** *567*, 67-72.

61. Peng, C.; Schlegel, H. B. *Isr. J. Chem.* **1993,** *33* (4), 449-454.

62. Gonzalez, C.; Schlegel, H. B. *J. Phys. Chem.* **1990,** *94* (14), 5523-5527.

63. Curtiss, L. A.; Raghavachari, K.; Redfern, P. C.; Pople, J. A. *J. Chem. Phys.* **1997,** *106* (3), 1063-1079.

64. Dunning Jr, T. H. *J. Chem. Phys.* **1989,** *90* (2), 1007-1023.

65. Blake, A. J.; Brain, P. T.; McNab, H.; Miller, J.; Morrison, C. A.; Parsons, S.; Rankin, D. W. H.; Robertson, H. E.; Smart, B. A. *J. Phys. Chem.* **1996,** *100* (30), 12280-12287.

66. Brain, P. T.; Morrison, C. A.; Parsons, S.; Rankin, D. W. H. *Dalton Trans.* **1996,** (24), 4589-4596.

67. Mitzel, N. W.; Rankin, D. W. H. *Dalton Trans.* **2003,** (19), 3650-3662.

68.   Gillespie, R. *J. Chem. Educ.* **1963,** *40* (6), 295.

69.   Bader, R. F.; Gillespie, R. J.; MacDougall, P. J. *J. Am. Chem. Soc.* **1988,** *110* (22), 7329-7336.

70.   Gillespie, R. J.; Robinson, E. A. *Angew. Chem. Int. Ed.* **1996,** *35* (5), 495-514.

71.   Hargittai, I.; Menyhárd, D. K. *J. Mol. Struct.* **2010,** *978* (1), 136-140.

72.   Atkinson, S. J.; Noble-Eddy, R.; Masters, S. L. *J. Phys. Chem. A.* **2016,** *120* (12), 2041-2048.

73.   Sipachev, V. A. *Struct. Chem.* **2000,** *11* (2), 167-172.

74.   Haaland, A. *Angew. Chem. Int. Ed.* **1989,** *28* (8), 992-1007.

75.   Shishkov, I.; Vilkov, L.; Pyatakov, N. *J. Struct. Chem.* **1992,** *33* (1), 38-42.

76.   Borisenko, K.; Samdal, S.; Shishkov, I.; Vilkov, L. *Acta Chem. Scand.* **1998,** *52*, 312-321.

77.   Pfafferott, G.; Oberhammer, H.; Boggs, J. E. *J. Am. Chem. Soc.* **1985,** *107* (8), 2309-2313.

78.   Shlykov, S. A.; Phien, T. D.; Gao, Y.; Weber, P. M. *Struct. Chem.* **2015,** *26* (5-6), 1501-1512.

79.   Nguyen, M. T.; Nguyen, V. S.; Matus, M. H.; Gopakumar, G.; Dixon, D. A. *J. Phys. Chem. A.* **2007,** *111* (4), 679-690.